

CHAPTER 1

INTRODUCTION

The title of this research is CFD of Double-wedge Spiked Intake of Supersonic Jet Engine. In this section, a brief introduction on the supersonic air intake of the jet engine will be discussed. The problem statement, objectives, scope of study and significance of work will be covered as well.

1.1 BACKGROUND

A jet engine is a reaction engine that discharges a fast moving jet of fluid to generate thrust in accordance with Newton's laws of motion. This broad definition of jet engines includes turbojets, turbofans, rockets, ramjets, pulse jets and pump-jets. In general, most jet engines are internal combustion engines but non-combusting forms also exist.

For this project, the scope will be the inlet of the supersonic jet engine. The design of the inlet of the supersonic jet engine is vital in the performance of the engine. It affects the efficiency of the engine and also affects the stability of the engine of the jet engine. At present, the supersonic jet engine requires a subsonic flow at the entry of the compressor, approximately 0.3 to 0.5 Mach number. However, in the process of slowing down the air entering the engine, there will be pressure losses which will highly affect the performance of the supersonic jet engine. Thus, the air intake must be designed in a way that the velocity of the air reduces yet keeping the pressure loss to a minimum amount.

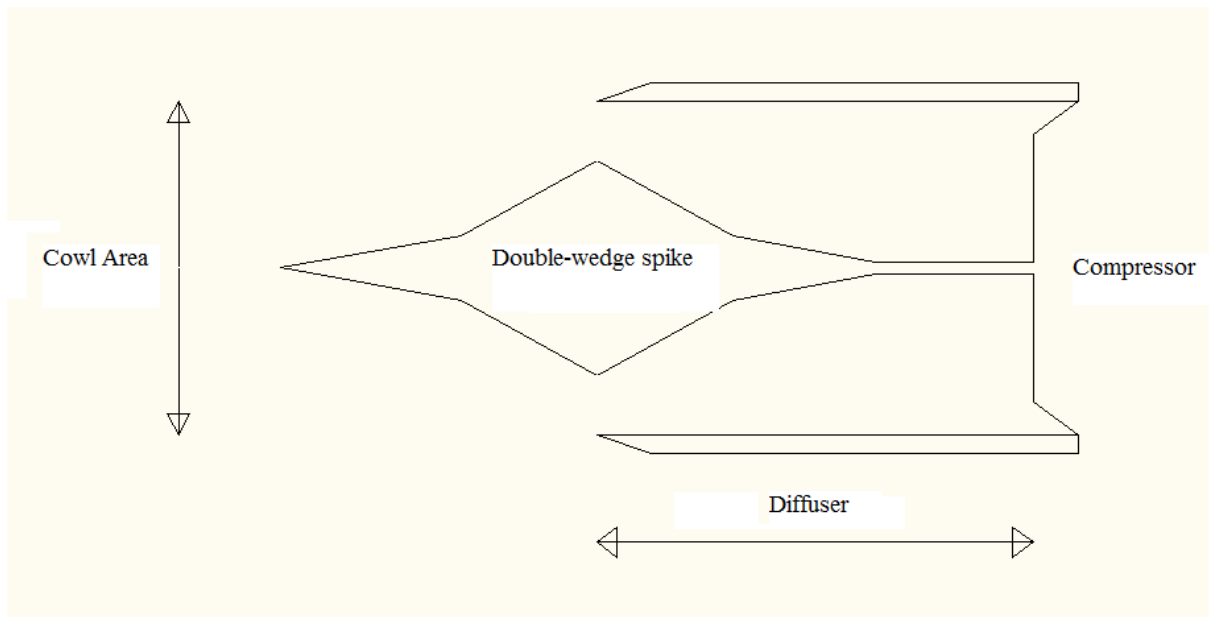


Figure 1.1: Simple Intake

The air intake of the supersonic jet engine consists of two main parts which is the spike and the subsonic diffuser shown in Figure 1.1.

1.2 PROBLEM STATEMENT

In a supersonic jet engine, the shock wave system and mass flow rate are influenced by the spike and the diffuser. The diffuser creates the normal shock wave where else the spike creates the oblique shock wave. The non -zero incidence angle changes the effective deflection angle of the shock wave at the upper and the lower side of the spike. Thus, the combining effect of the incidence and fore body angles is essential for the intake performance of the supersonic jet engine.

1.3 OBJECTIVES

The objectives of this research are:

- To model mathematically the double-wedge spiked intake of the supersonic jet engine.
- To simulate the spiked intake of the supersonic jet engine by the CFD technique.
- To investigate the flow characteristics at various design and operational conditions.
- To investigate the strength of CFD software. (FLUENT)

1.4 SCOPE OF STUDY

In this research, there are three scope of studies required. First is the mathematical modelling of the exterior and interior part of the supersonic intake. The governing equations of this system will be set up and an analytical modelling will be done.

Next, Computational Fluid Dynamics technique will be used to simulate the flow characteristics at the double-wedge spiked intake of the supersonic jet engine. The results from the simulation will be verified with the numerical works and also experimental work.

Finally, a simulation and analysis will be done on the double-wedge spiked intake at different angle of attack and Mach number.

1.5 SIGNIFICANCE OF THE WORK

High efficiency, performance and the stability of the supersonic gas engine is a crucial criteria of a supersonic jet engine. The change of the speed and angle of attack, the pressure distribution of the diffuser part in the leeside and the windward side will be highly effected. The difference in pressure distribution in the leeside and windward side will hence affect the performance of the air compression in the gas turbine engine. In addition to that, if the difference in the pressure distribution between the two sides of the compressor is too high, it will cause the engine to halt or cause mechanical failure.

The present research is to investigate the usage of the double-wedge spiked intake in the supersonic jet engine will influence the pressure distribution and the flow characteristics at the diffuser part of the supersonic jet engine. Further research and modifications can be done in the intake to improve the efficiency of the supersonic jet engine or to provide more information to the operator on the unfavourable region of the operation for continuous safety flight. In addition, the reliability of the supersonic jet engine can be increased with the avoidance of mechanical failure.

CHAPTER 2

LITERATURE REVIEW

A spike is a wedge or cone shaped body which is positioned at the supersonic jet engine intake with the main purpose of creating a series of shocks outside at the inlet of the jet engine.[7] A double wedge spike is a spike which has double wedges in the spike. This is to create a double oblique shock wave system. For this stationary spike, the geometry is fixed thus leading to a fixed throat area. In contrary, there is an also movable spike which is able to provide a variable geometry intake. This type of intakes are required to produce a throat area which is large enough for the establishment of supersonic flow and, which can subsequently be reduced to provide efficient wedge compression in the running condition.[7]

With usage of the double wedge spiked intake, the deceleration of the flow intake are conducted in stages instead of just a single step (as by only with the normal shock wave). [7] With the implementation of double wedge spike at the inlet, three shock waves will be created, the first oblique shock wave, the second oblique shock wave and then followed by the normal shock wave. The geometry of the spikes determines the number of shock waves created. Each corner of the geometry would result in a shock wave each, be it the oblique or the normal shock wave.

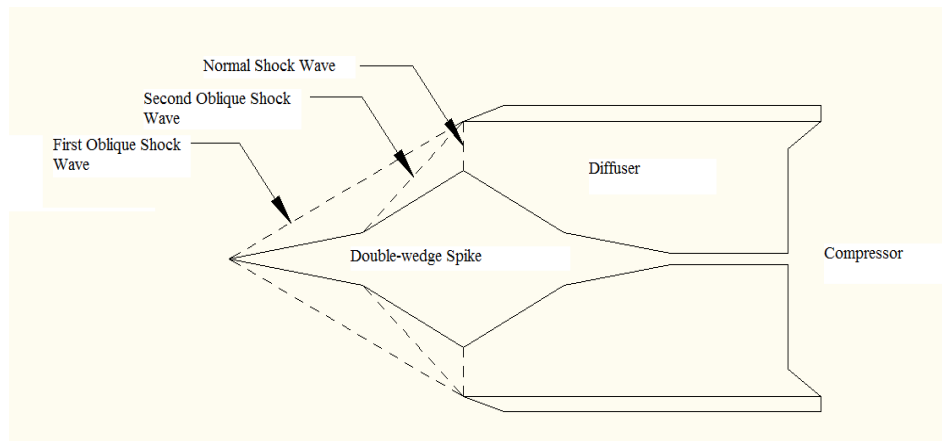
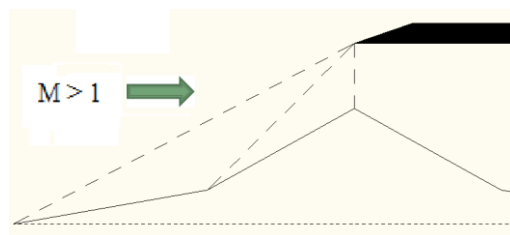


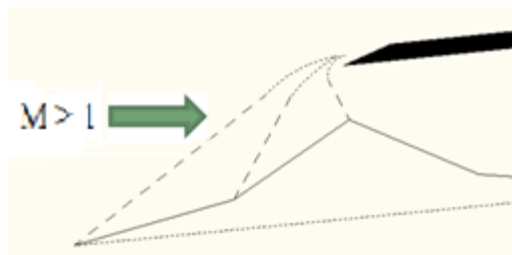
Figure 2.1: Supersonic intake with Two Deflection Feature

The shock wave system will be affected in three different operational situations, which are the critical, subcritical and the supercritical modes. The critical operation system happens when the shock waves meet exactly at the diffuser throat. At this point, the cross section is minimal resulting in a maximum rate of airflow and a minimal loss of stagnation pressure.

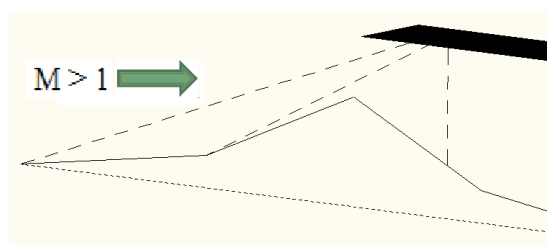
Sub-critical operation system occurs when the shock waves moves upstream to the duck entry. This condition is highly unstable and will produce shock oscillating at a high rate near the intake. The supercritical operation system occurs when the shock waves moves downstream into the throat, which will result in a poor flow quality.



(a) Critical



(b) Sub-critical (windward-side)

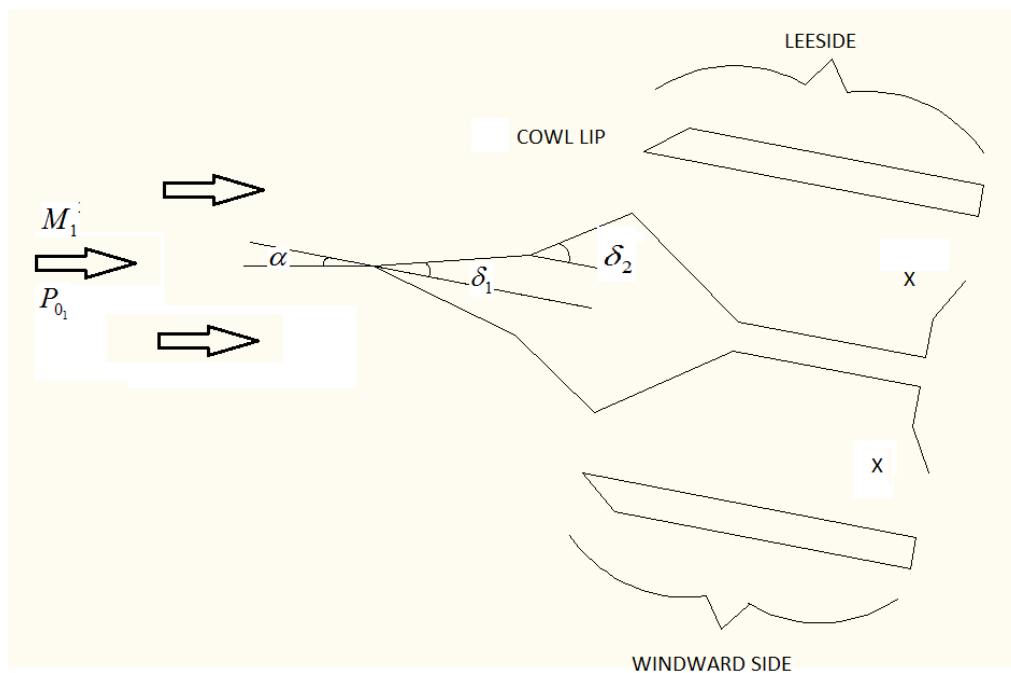


(c) Supercritical (lee side)

Figure 2.2: Supersonic Intake-Modes of Operation

The supersonic jet engine performance is affected by two factors which are the angle of attack and the spike geometry.

Different type of shock system will be experienced, which is the leeside and windward side when the angle of attack changes. When the angle of attack is more than zero, the oblique shock on the leeside will experience smaller shock angle, thus experiencing supercritical conditions. Whereas in the windward side, the deflection angle of the shock wave is larger and consequently, the variation of properties is larger than in the leeside.[3]



X= location of P/P_{0_1}

Figure 2.3: Outline of 2-dimensional inlets

2.1 LITERATURE SURVEY

Beastall (1953) presented the certain types of flow instability that occur with the centre-body diffuser at the supersonic speed. An experimental work has been suggested to provide data in designing diffuser which are stable with regards to large and small oscillation. Experimental work suggested that wind tunnel test should be done with different wedge angle and different position of centre body with a given Mach number. Limits of position of centre body for unstable flow can be found and hence with this information it is possible to design a diffuser which is stable. Further testing are still required as although a diffuser may be stable with regards to large oscillation it may still be vulnerable to small oscillations.[2]

S.S. Gokhale and V.R. Kumar (2001) used the compressible Navier-Stokes equations in two dimensions without body force or external heat addition as the governing equation. The Baldwin-Lomax turbulence model is used to simulate the effects of fine scale turbulence. A Prandtl-Van Driest formulation is used in the inner region and the Clauser formulation with Klebanoff intermittence function is used in the outer region.

A 151*91 grid with clustering near the wall region is used to predict the pressure in the duct region. For Scramjet, the inlet Mach of 3.0 and 2.5 with same geometry is considered in the study. From the isoMach contour plot is show for both Mach number, the flow in the duct is shock free as only isentropic compression takes place followed by compression due to cowl shock impinging on the lower wall.

The code created is capable of predicting all complex inlet flow features (shock due to forebody, multiple shock reflection, normal shock, shock boundary, layer introduction and associated separation for two dimensional and axis-symmetric inlets and computed values are in good agreement with the experimental data available. The code can be used to study supersonic inlet performance under off-design operating conditions. [3]

Salih (2003) carried out an analysis on the effect of angle of attack on the shock system in the single wedge and double wedged spikes in the pressure recovery in the inlet of compressor. The analysis is carried out by dividing the intake into 2 parts; the external part (the shock wave system) and the internal (subsonic diffuser). The external part (shock wave system) is

modelled and analysed analytically. The flow in the subsonic diffuser part is considered perfect, non viscous into dimensional. The set of governing equation is to be solved by Patankar method called 'SIMPLE'. The preliminary program was designed to state the inlet boundary conditions by taking into account the shock system and the inlet of the intake. Study was done on the pressure recovery behaviour with the change in angle of attack (from 0-10) at different flying Mach numbers (1.8 and 2.2) for single wedge and double wedge spike. ($\delta_1=6^\circ$, $\delta_2=4^\circ$, $\delta_3=6^\circ$)

The flow assumption of viscous flow is necessary to be taken into consideration as different results are obtained than that of non-viscous flow assumption. The results obtained from the numerical analysis are in agreement with those obtained experimentally by previous researches.[4]

Thangadurai and Chandra (2003), solved governing equations and boundary conditions using the flow simulation software FLUENT. Finer grids were used in the steep-gradient zones, such as boundary layers near the walls and also at the locations of normal and oblique shocks. The conservation equations for mass, momentum, energy and turbulence quantities are solved using the finite volume technique. The results from the numerical analysis are then validated by comparing with the experimental data.

Axisymmetric and two-dimensional supersonic mixed compression air intake of realistic configuration has been studied. For axisymmetric mixed compression, the predicted cowl inner wall static pressure and pressure recovery show good agreement with the experimental data. As for the two-dimensional mixed compression, the prediction of static pressure variation along the cowl inner surface and ramp outer surface show good agreement with the experimental data as well.

From the results of the numerical simulation also, heat addition significantly increases the pressure recovery along the cowl inner surface and centre body. The model developed by the author to predict the flow in air intake is able to capture the flow features such as shock pattern and pressure recovery. The flow model developed can be used effectively to predict the flow environment in generic intake.[5]

Jain and Mittal (2005) performed a numerical simulation of 2D mixed compression supersonic inlet by solving unsteady compressible Euler equation via a stabilized finite element method.

Numerical computations were performed for various back pressures with same inlet geometry. As the back pressure increases, the normal shock wave converged to the convergent part. Computations were also done for different geometries, with all intakes having same length and throat area but different length at the second ramp.

The conclusion from the study is that the critical pressure and corresponding pressure recovery is higher for inviscid flow. The variation between total pressure recovery and back pressure is almost linear. It was also found that in addition to the throat-to-inlet area ration, the ramp geometries plays an important role in the start-up dynamics. [9]

Al-Kayiem & Aboud (2007) carried out an analysis of the flow field in the supersonic spike intake by subdivided in into three different regions. The first and second regions which are the flow across oblique shock wave and across normal shock wave are predicted by analytical simulation using the related governing equations. The equations are solved under different operating conditions and results after the normal shock wave is used as inlet conditions for the internal part of the intake, The internal part of the intake is analysed by CFD technique based on finite difference approximation. The solution is carried out numerically under assumption of 2-D, compressible and non-viscous. The nodal network was re-mapped by using a rectangular computational nodal network to represents the complex physical domain.

The results are obtained for different operating condition at incidence angles (0° , 4° , 8° , 12° , 16° , 20°). Mach number is varied from 1.3 to 3. The entire analysis is carried out with two different spike deflection angles (6° and 12°). The total pressure recovery is the main parameter for comparison at different conditions.

From the results the total pressure recovery evaluation demonstrates considerable variation in the pressure forces at the compressor inlet. The angle of attach and spike angle contributes effectively in the flow structure and resulting in pressure in the compressor inlet.[6]

Tan Kien Weng(2009), did a study on the simulation and flow characterization of spiked supersonic gas turbine intake at non-zero angle of attack.

The inlet part of the intake, shock modelling was done using analytical method, whereas the diffuser area was solved using numerical method. The improvisation was done on the pressure recovery which included the consideration of turbulence flow. It was noticed that at Mach No 1.4, as the angle of attack increases from 2° , the pressure recovery decreases and becomes constant. At low Mach number, the deflection angle increases and exceeded the deflection angle, which will eventually lead to detached shock wave.

From the numerical analysis, it showed that the pressure recovery degrades at the leeward side with the increase of the angle of attack and increases at the windward side. By increasing the Mach number, the pressure recovery will decrease at both sides.[7]

CHAPTER 3

THEORY OF COMPRESSIBLE FLUID

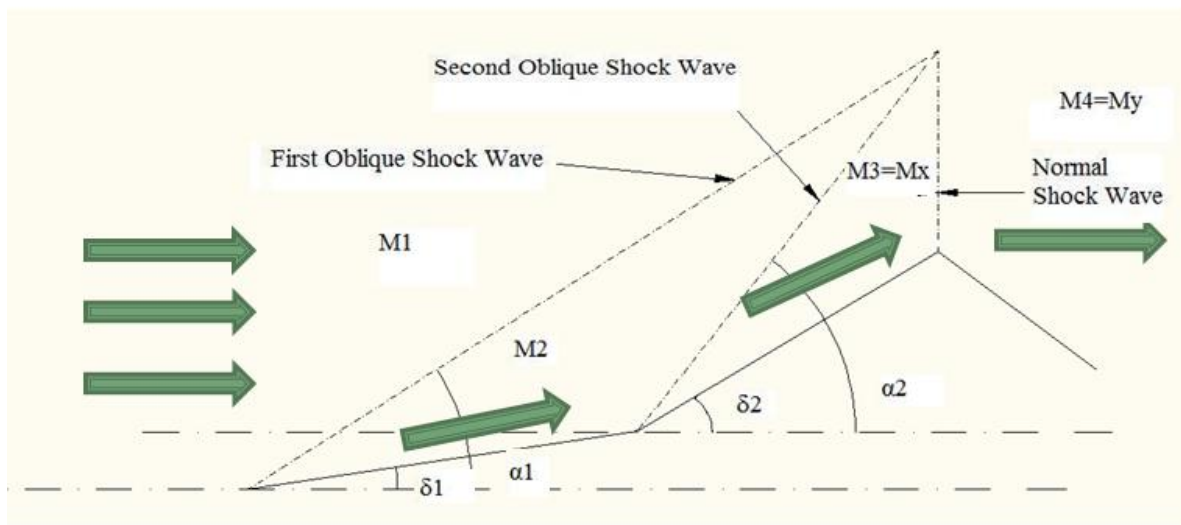


Figure 3.1: Shock waves at the inlet

The following assumptions are used in this study:

1. Constant pressure specific heat, $C_p = 1.005 \text{ kJ/kg.K}$
 Specific heat ratio, $k = 1.4$
 Gas constant, $R = 0.287 \text{ kJ/kg.K}$

Compressible fluid has variable density, which can be derived from the equation of state shown below:

$$\rho = \frac{P}{RT} \quad (3.1)$$

and the velocity at any point can be denoted by:

$$V = Ma \quad (3.2)$$

where

$$a = \sqrt{kRT} \quad (3.3)$$

2. The flow is isentropic through the external flow except through the shock layer which is adiabatic
3. The flow field in the diffuser region is to be considered as 2-dimensional, steady and viscous. ($\mu = \text{constant}$)
4. The spike has a fixed geometry.
5. Free stream properties (T^∞ , P^∞) depend on the altitude of the aircraft (H). [for this study the flight height is assumed at 10 000m] as in these relations:

$$T^\infty = 288.16 - 0.0065H \quad (3.4)$$

$$P^\infty = 101325 \left(\frac{T^\infty}{288.16} \right)^{\frac{0.03415H}{288.16 - T^\infty}} \quad (3.5)$$

3.1 MODELLING OF SHOCK SYSTEM

3.1.1 Isentropic Flow

The isentropic flow is characterized by frictionless and adiabatic flow. As in this study, the local Mach number is the reference or the characteristics parameter. The velocity (Mach number) changes with the flow area. This would result in changes in the properties of the local flow, which can be evaluated as below:

$$\text{Pressure ratio:} \quad \frac{P_0}{P} = \left[1 + \frac{k-1}{2} M^2 \right]^{\frac{k}{k-1}} \quad (3.6a)$$

$$\text{Density ratio:} \quad \frac{\rho_0}{\rho} = \left[1 + \frac{k-1}{2} M^2 \right]^{\frac{k}{k-1}} \quad (3.6b)$$

$$\text{Temperature ratio:} \quad \frac{T_0}{T} = \left[1 + \frac{k-1}{2} M^2 \right] \quad (3.6c)$$

3.1.2 Modelling of the First Oblique Shock Wave

$$\tan \delta_1 = \frac{2 \cot \sigma_1 (M_1^2 \sin^2 \sigma_1 - 1)}{2 + M_1^2 (k + \cos 2\sigma_1)} \quad (3.7a)$$

Downstream Mach No.

$$M_2 = \sqrt{\frac{(k-1)M_1^2 \sin^2 \sigma_1 - 2}{2kM_1^2 \sin^2 \sigma_1 - (k-1) \sin^2 \sigma_1} \frac{1}{\sin^2(\sigma_1 - \delta_1)}} \quad (3.7b)$$

Pressure ratio

$$\frac{P_2}{P_1} = \frac{2k}{k+1} M_1^2 \sin^2 \sigma_1 - \frac{k-1}{k+1} \quad (3.7c)$$

Density ratio

$$\frac{\rho_2}{\rho_1} = \frac{(k+1)M_1^2 \sin^2 \sigma_1}{2 + (k-1)M_1^2 \sin^2 \sigma_1} \quad (3.7d)$$

Temperature ratio

$$\frac{T_2}{T_1} = \left(\frac{2k}{k+1} M_1^2 \sin^2 \sigma_1 - \frac{k-1}{k+1} \right) \left(\frac{2 + (k-1)M_1^2 \sin^2 \sigma_1}{(k+1)M_1^2 \sin^2 \sigma_1} \right) \quad (3.7e)$$

Total Pressure Ratio

$$\frac{P_{0_2}}{P_{0_1}} = \frac{P_2}{P_1} \left(\frac{1 + \frac{k-1}{2} M_2^2}{1 + \frac{k-1}{2} M_1^2} \right)^{\frac{k}{k-1}} \quad (3.7f)$$

3.1.3 Modelling of the Second Oblique Shock Wave

$$\tan \delta_2 = \frac{2 \cot \sigma_2 (M_2^2 \sin^2 \sigma_2 - 1)}{2 + M_2^2 (k + \cos 2\sigma_2)} \quad (3.8a)$$

Downstream Mach No.

$$M_3 = \sqrt{\frac{(k-1)M_2^2 \sin^2 \sigma_2 - 2}{2kM_2^2 \sin^2 \sigma_2 - (k-1)\sin^2 \sigma_2} \frac{1}{\sin^2(\sigma_2 - \delta_2)}} \quad (3.8b)$$

Pressure ratio

$$\frac{P_3}{P_2} = \frac{2k}{k+1} M_2^2 \sin^2 \sigma_2 - \frac{k-1}{k+1} \quad (3.8c)$$

Density ratio

$$\frac{\rho_3}{\rho_2} = \frac{(k+1)M_2^2 \sin^2 \sigma_2}{2 + (k-1)M_2^2 \sin^2 \sigma_2} \quad (3.8d)$$

Temperature ratio

$$\frac{T_3}{T_2} = \left(\frac{2k}{k+1} M_2^2 \sin^2 \sigma_2 - \frac{k-1}{k+1} \right) \left(\frac{2 + (k-1)M_2^2 \sin^2 \sigma_2}{(k+1)M_2^2 \sin^2 \sigma_2} \right) \quad (3.8e)$$

Total pressure ratio

$$\frac{P_{0_3}}{P_{0_2}} = \frac{P_3}{P_2} \left(\frac{1 + \frac{k-1}{2} M_3^2}{1 + \frac{k-1}{2} M_2^2} \right)^{\frac{k}{k-1}} \quad (3.8f)$$

3.1.4 Modelling of Normal Shock Wave

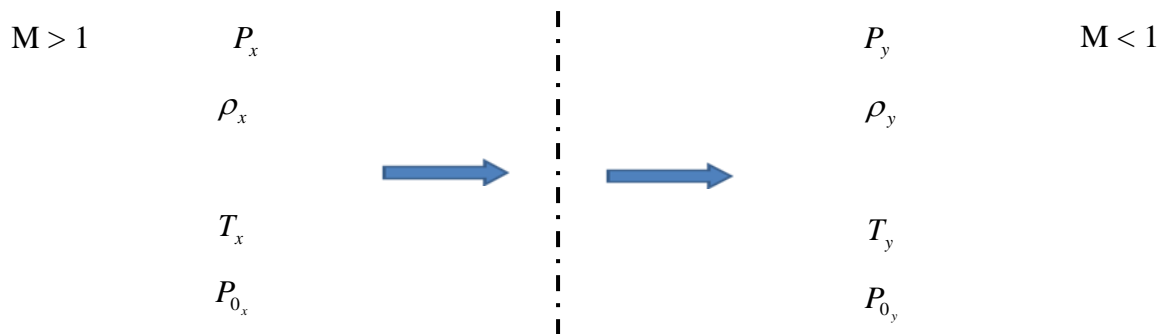


Figure 3.2: Normal Shock Wave

Downstream Mach No

$$M_y = \sqrt{\frac{(y-1)M_x^2 + 2}{2kM_x^2 - (k-1)}} \quad (3.9a)$$

Pressure ratio

$$\frac{P_y}{P_x} = \frac{2k}{k+1} M_x^2 - \frac{k-1}{k+1} \quad (3.9b)$$

Density ratio

$$\frac{\rho_y}{\rho_x} = \frac{(k+1)M_x^2}{2 + (k-1)M_x^2} \quad (3.9c)$$

Temperature ratio

$$\frac{T_y}{T_x} = \left(\frac{2k}{k+1} M_x^2 - \frac{k-1}{k+1} \right) \left(\frac{2 + (k-1)M_x^2}{(k+1)M_x^2} \right) \quad (3.9d)$$

Total pressure ratio

$$\frac{P_{0_y}}{P_{0_x}} = \left(\frac{2k}{k+1} M_x^2 - \frac{k-1}{k+1} \right)^{\frac{-1}{k-1}} \left(\frac{(k+1)M_x^2}{2 + (k-1)M_x^2} \right)^{\frac{k}{k-1}} \quad (3.9e)$$

3.1.5 Modelling of detached shock wave

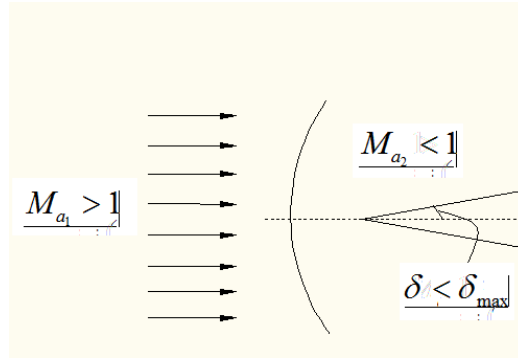


Figure 3.3: Detached Shock Wave

Detached shock wave is the shock wave that is created with no contact with the body it originated from. This type of shock wave is created when the flow passes the wedge with deflection angle greater than the maximum deflection angle.

δ_{\max} can be found using

$$\tan \delta_{\max} = \frac{2 \cot \sigma_{\max} (M_1 \sin^2 \sigma_{\max} - 1)}{2 + M_1^2 (k + \cos 2\sigma_{\max})} \quad (3.10a)$$

where σ_{\max} can be found from

$$\sin^2 \sigma_{\max} = \frac{k+1}{4k} - \frac{1}{kM_1^2} \left[1 - \sqrt{(k+1) \left(1 + \frac{k-1}{2} M_1^2 + \frac{k+1}{16} M_1^4 \right)} \right] \quad (3.10b)$$

3.1.6 Prandtl-Meyer Waves Modelling

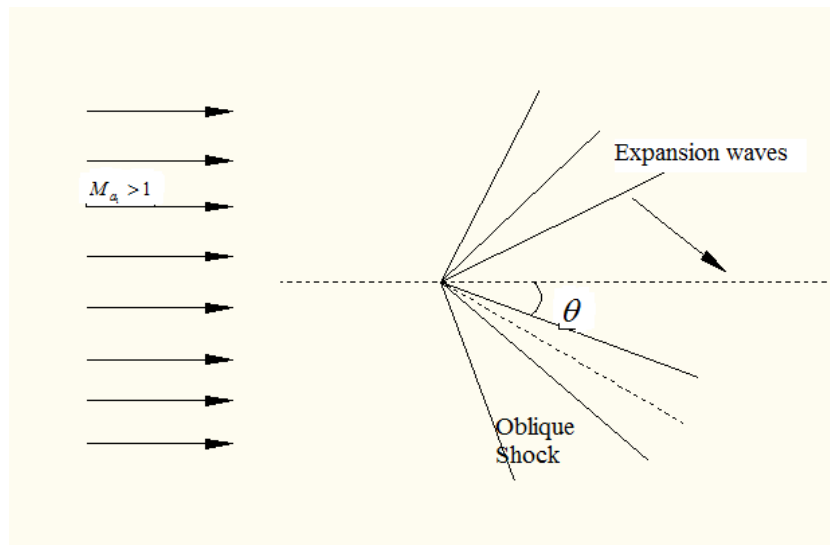


Figure 3.4: Prandtl-Meyer Wave

When the angle of attack becomes higher than the wedge deflection angle, the flow becomes expanded, rather than compressed in other scenarios. This type of expansion is known as the Prandtl-Meyer Expansion Waves. The change in properties occurs gradually across a series of waves occurring on the surface.

The turning angle:

$$\theta = v_2 - v_1 \quad (3.11a)$$

Where $v=f(M)$

$$v = \sqrt{\frac{k+1}{k-1}} \tan^{-1} \sqrt{\frac{k-1}{k+1} (M^2 - 1)} - \tan^{-1} \sqrt{M^2 - 1} \quad (3.11b)$$

The change of properties across these waves are isentropic which means the stagnation temperature and pressure, T_0 and P_0 are constants.

3.2 MODELLING DIFFUSER FLOW

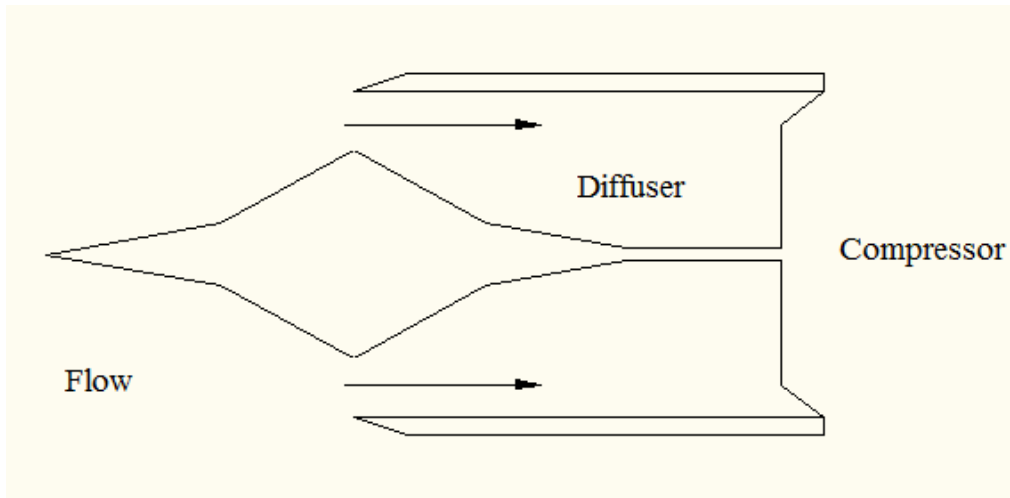


Figure 3.5: Diffuser part of the intake

The flow properties inside the diffuser can be solved numerically. For the modelling of the diffuser flow, a few assumptions are taken into account, which are:

- The flow is steady, $\frac{\delta}{\delta t} = 0$
- The fluid is viscous, $\mu \neq 0$
- There is no body force, $\rho g = 0$
- The flow is compressible, $\rho = \frac{P}{RT}$
- 2-dimensional flow

Thus the Navier-Stokes equation which is the governing equation of the flow becomes

The continuity equation

$$\left[\frac{\partial(\rho u)}{\partial x} + \frac{\partial(\rho v)}{\partial y} \right] = 0 \quad (3.12a)$$

X-momentum

$$u \frac{\partial u}{\partial x} + v \frac{\partial u}{\partial y} + \frac{1}{\rho} \frac{\partial P}{\partial x} = \frac{\mu}{\rho} \left(\frac{\partial^2 u}{\partial x^2} + \frac{\partial^2 u}{\partial y^2} \right) \quad (3.12b)$$

Y-momentum

$$u \frac{\partial v}{\partial x} + v \frac{\partial v}{\partial y} + \frac{1}{\rho} \frac{\partial P}{\partial y} = \frac{\mu}{\rho} \left(\frac{\partial^2 v}{\partial x^2} + \frac{\partial^2 v}{\partial y^2} \right) \quad (3.12c)$$

Energy Equation

$$\frac{\partial \left(\rho \left(e + \frac{V^2}{2} \right) u \right)}{\partial x} + \frac{\partial \left(\rho \left(e + \frac{V^2}{2} \right) v \right)}{\partial y} = \frac{\partial}{\partial x} \left(k \frac{\partial T}{\partial x} \right) + \frac{\partial}{\partial y} \left(k \frac{\partial T}{\partial y} \right) + \frac{\partial}{\partial x} (-up + u\tau_{xx} + v\tau_{xy}) + \frac{\partial}{\partial y} (-vp + u\tau_{yx} + v\tau_{yy}) \quad (3.12d)$$

3.3 TURBULENCE MODELLING

The turbulence flow in this study will be simulated by using the standard k-epsilon model with enhanced wall treatment. In this model, two additional transport equations are being solved which are the turbulence kinetic energy, k and the turbulence dissipation rate, ϵ . The turbulence viscosity is then computed as a function of k and ϵ .

The turbulence kinetic energy, k and turbulence dissipation rate, is obtained from

$$\frac{\partial}{\partial t} (\rho k) + \frac{\partial}{\partial t} (\rho k u_i) = \frac{\partial}{\partial x_j} \left[\left(\mu + \frac{\mu_t}{\sigma_k} \right) \frac{\partial k}{\partial x_j} \right] + G_k + G_b - \rho \epsilon - Y_M - S_k \quad (3.13a)$$

and

$$\frac{\partial}{\partial t} (\rho \epsilon) + \frac{\partial}{\partial x_i} (\rho \epsilon u_i) = \frac{\partial}{\partial x_j} \left[\left(\mu + \frac{\mu_t}{\sigma_\epsilon} \right) \frac{\partial \epsilon}{\partial x_j} \right] + C_{1\epsilon} \frac{\epsilon}{k} (G_k + C_{3\epsilon} G_b) + C_{2\epsilon} \rho \frac{\epsilon^2}{k} + S_\epsilon \quad (3.13b)$$

where,

G_k = generation of turbulence kinetic energy due to mean velocity gradients

G_b = generation of turbulence kinetic energy due to buoyancy

Y_M = contribution of the fluctuating dilatation in compressible turbulence to the overall dissipation rate

The turbulent viscosity, μ_t is computed by combining k and ε as below:

$$\mu_t = \rho C_\mu \frac{k^2}{\varepsilon} \quad (3.13c)$$

where C_μ is a constant.

The values of the constants in the equations which is the default values set by FLUENT, are as follows:

$$C_{1\varepsilon} = 1.44$$

$$C_{2\varepsilon} = 1.92$$

$$C_\mu = 0.09$$

$$\sigma_k = 1.0$$

$$\sigma_\varepsilon = 1.3$$

These values have been determined experimentally and have been found to work fairly well for wide range of wall-bounded and free shear flow.

CHAPTER 4

METHODOLOGY

4.1 TECHNIQUES OF ANALYSIS

The analysis will be conducted by a few methods:

- a. A mathematical modelling of the double-wedge spiked intake of the supersonic jet engine will be created.

- b. The whole system, which is the exterior and interior part of the inlet of supersonic jet engine, will be simulated using CFD technique. This will be done using softwares which are GAMBIT and FLUENT.

- c. Finally, the flow characteristics will be investigated at various design and operational conditions. This will be done by changing the angle of attack and changing the Mach number at the inlet.

4.2 GANTT CHART AND MILESTONE

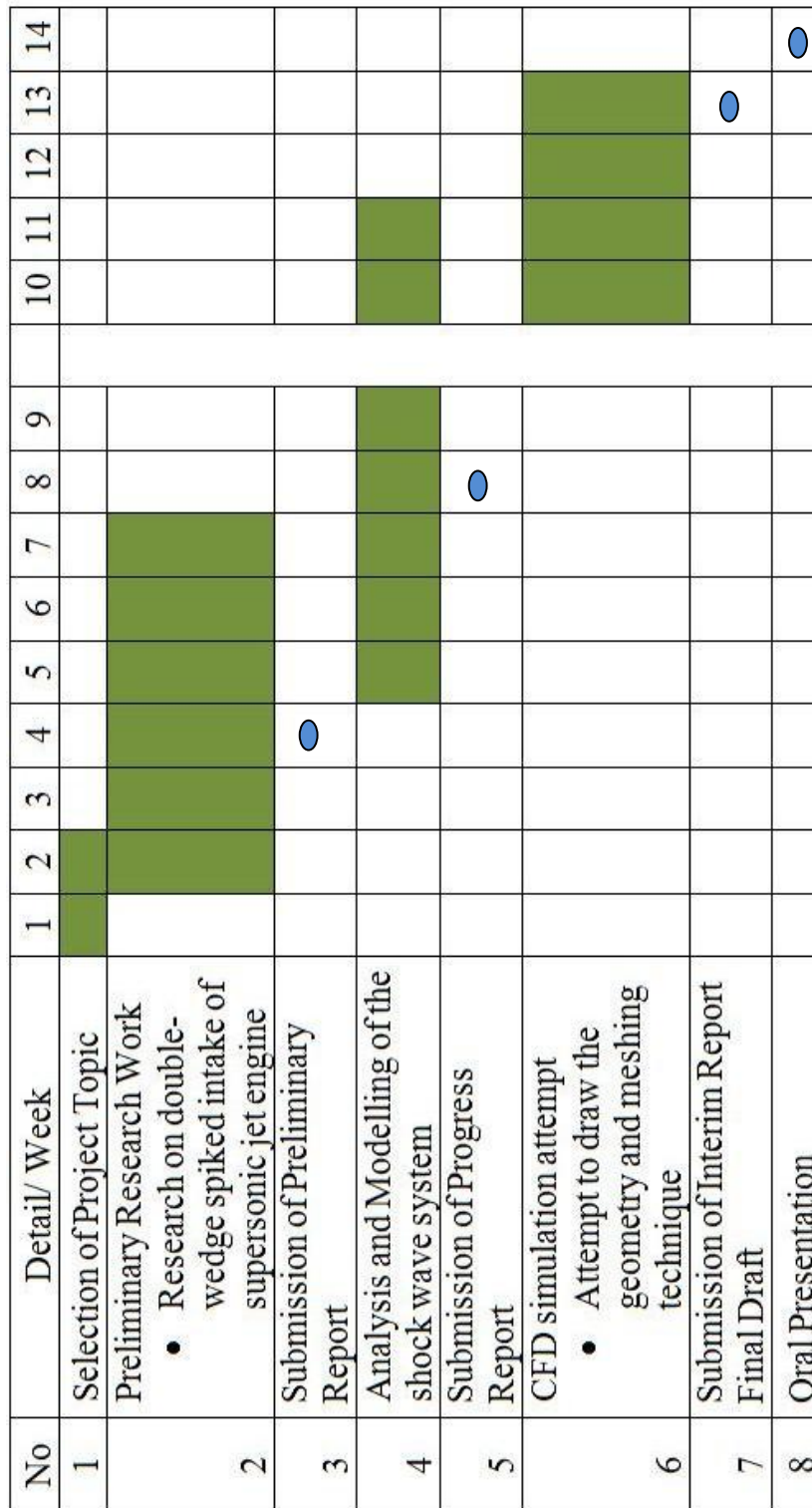


Figure 4.1: Gantt Chart and Milestone

- Milestone
- █ Process

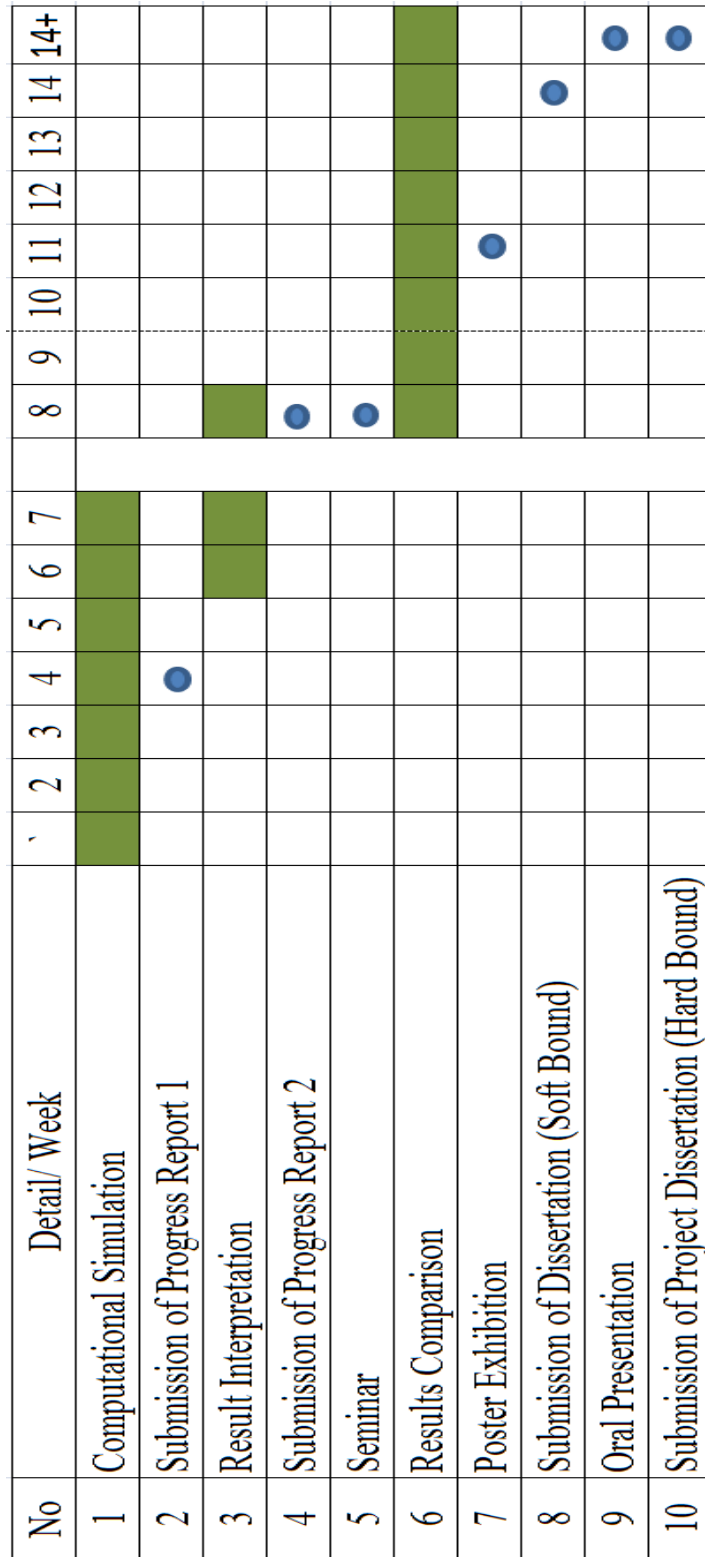


Figure 4.2: Gantt Chart and Milestone

● Milestone
 ■ Process

4.3 EXECUTION FLOW CHART

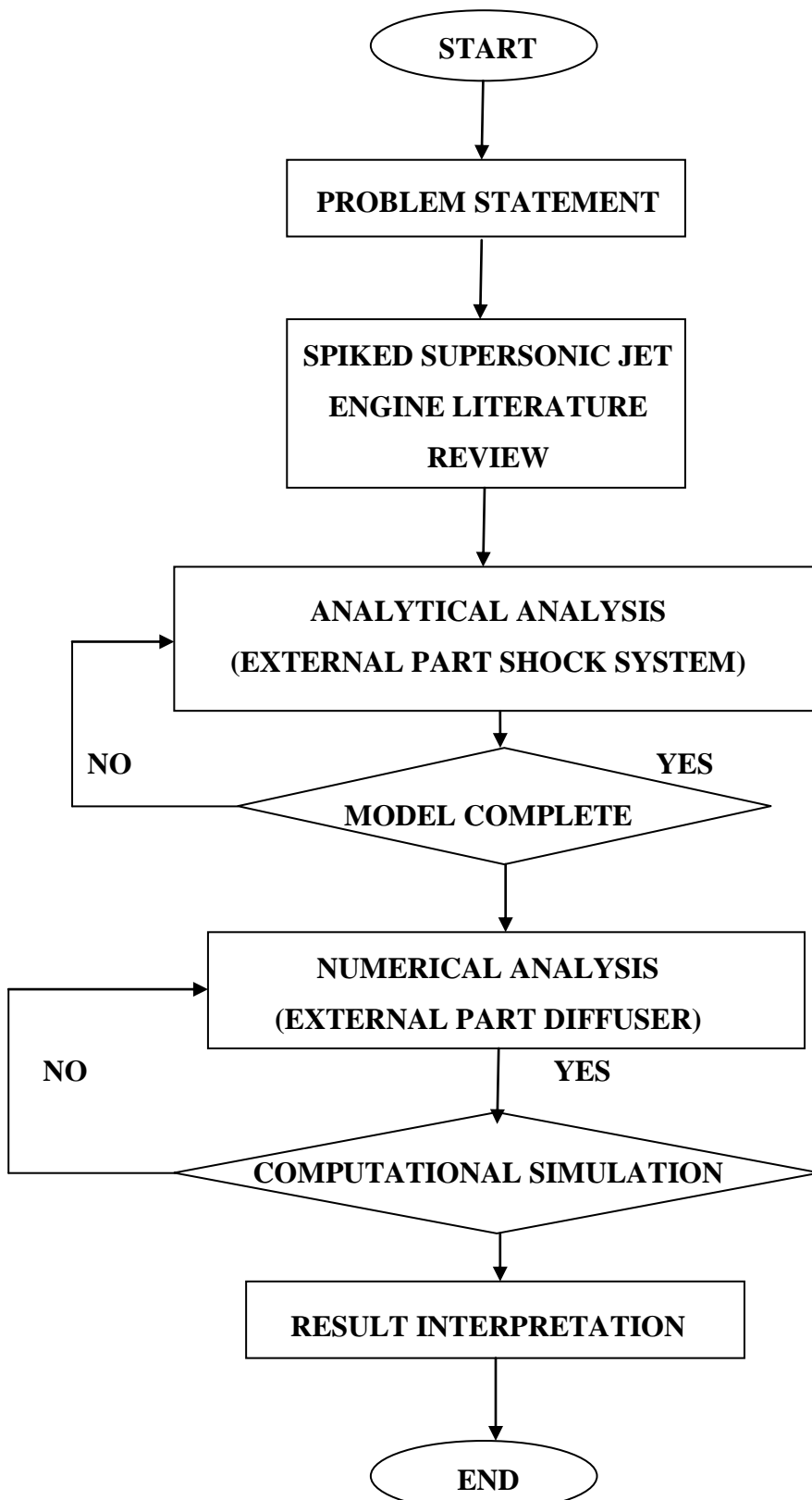


Figure 4.3: Execution Flow Chart

4.4 REQUIRED EQUIPMENT AND SOFTWARE

There will be two softwares used for this project

- a. GAMBIT
- b. FLUENT
- c. Microsoft Office Excel 2007
- d. MATLAB

The software in the department will be used to simulate the system.

CHAPTER 5

ANALYTICAL ANALYSIS

The analytical analysis of the flow has been carried out using several programs. The results were tabulated and plotted to see the pattern and the changes.

For the leeside, equations 3.7, 3.8 and 3.9 was used to compute the properties and for the windward side an addition of equation 3.10 is used. The initial values are computed as follows:

Inlet Mach No, $M_1 = 1.4 - 3.0$

Angle of attack, $\alpha = 0^\circ, 6^\circ, 12^\circ$

Height of flight, $H = 10\ 000\text{m}$

Specific heat ratio, $k = 1.4$

Therefore, using equation 3.1, 3.4 and 3.5, the Density, Temperature and Pressure are as follows:

$$T_1 = 223.16\ \text{K}$$

$$P_1 = 26451.4\ \text{Pa}$$

$$\rho_1 = 47.04\ \text{kg/m}^3$$

Then using equation 3.7, 3.8, 3.9, 3.10 and 3.11, the other calculations are done. Iteration method is used to solve equation 3.7a, 3.8a, and 3.11a and other are calculated analytically.

The calculations are shown in appendix.

5.1 RESULTS OF ANALYTICAL ANALYSIS

α	Ma1	Ma4	P4	ρ_4	T4	Po4
0	1.4	0.84263	52487.8	0.03716	375.536	11377476
6	1.4	1.03195	73435.7	0.04698	283.53	17895508
12	1.4	1.32983	62676.9	0.04165	151.994	21831110
0	1.8	0.69268	101361	0.0583	658.355	15757717
6	1.8	0.81269	93112.3	0.05575	474.222	20484259
12	1.8	0.84277	202645	0.09477	568.277	34556375
0	2.2	0.59454	170300	0.08005	1061.7	18100243
6	2.2	0.64474	180689	0.086	905.391	25023271
12	2.2	0.72182	176279	0.08556	724.488	32681602
0	2.6	0.53798	259700	0.10076	1543.81	19162156
6	2.6	0.51143	363624	0.12054	1982.96	20160198
12	2.6	0.62652	303118	0.1205	1141.68	41110431
0	3	0.50179	372676	0.12036	2108.21	19265238
6	3	0.52793	442052	0.14318	1914.32	31153773
12	3	0.56817	477306	0.15671	1650.9	47878115

Table 5.1: Results of analytical analysis for windward side

α	Ma1	Ma4	P4	ρ_4	T4	Po4
0	1.4	0.973	44912.2	0.03336	273.888	12599333
6	1.4	0.77043	61132.8	0.04128	463.104	10701787
12	1.4	0.68713	84067.9	0.05094	634.124	10167937
0	1.8	0.973	44912.2	0.03336	273.888	16936035
6	1.8	0.63223	108948	0.05983	813.032	12700463
12	1.8	0.58874	139357	0.06903	1025.71	11475114
0	2.2	0.73169	121617	0.06686	624.141	23254098
6	2.2	0.55721	171998	0.07737	1248.6	13523178
12	2.2	0.52703	218073	0.08719	1555.7	11541524
0	2.6	0.68522	167763	0.08295	780.984	29304438
6	2.6	0.51169	250669	0.09311	1768.03	13379865
12	2.6	0.48932	316497	0.10317	2188.2	10904279
0	3	0.65755	216896	0.09827	917.96	35828894
6	3	0.48111	348844	0.10741	2390.46	12538949
12	3	0.46355	442138	0.11777	2960.81	9788804.9

Table 5.2: Results of analytical analysis for leeside

5.2 VERIFICATION OF PROGRAM FOR ANALYTICAL ANALYSIS

The results of the analytical analysis have to be verified to ensure that the calculations are done properly. Therefore the results of the analytical analysis will be compared with oblique shock properties graph, normal shock properties graph and Prandtl-Meyer properties table respectively.

M_a	Shock Wave Angle (degrees)		Percentage error (%)
	Analytical Analysis for Oblique Shock	Oblique Shock Properties Graph	
1.4	52.9	51.5	2.72
1.8	40.0	41.0	2.44
2.2	33.2	32.1	3.42
2.4	29.0	28.2	2.84
3.0	26.1	25.3	3.16

Table 5.3: Result comparison for analytical analysis for zero angle of attack for oblique shock angle

	$Ma_3=1.8$		$Ma_3=2.6$	
	Analytical Analysis for N.S Wave	N.S. Properties Table	Analytical Analysis for N.S Wave	N.S. Properties Table
M_4	0.6165	0.6165	0.509	0.509
P_4/P_3	3.613	3.613	7.720	7.720
ρ_4/ρ_3	2.359	2.359	3.449	3.449
T_4/T_3	1.532	1.532	2.238	2.238
P_{o4}/P_{o3}	0.8127	0.8127	0.460	0.460

Table 5.4: Result comparison for analytical analysis for zero angle of attack for Normal Shock Wave

M_1	M_2	
	P-M Analytical Results	P-M Properties Table
1.5	2.208	2.208
2.0	2.831	2.831

Table 5.5: Result comparison for analytical analysis for Prandtl-Meyer Expansion Wave

CHAPTER 6

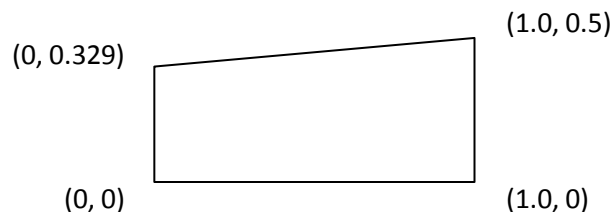
NUMERICAL ANALYSIS

There are two parts for numerical analysis. One is numerical analysis done for the diffuser part using the results obtained from the analytical analysis for the shock waves, and then the other one is the simulation of the whole system numerically. The results are then compared.

The modelling of the systems is done using GAMBIT and the numerical analysis is done using FLUENT.

6.1 MODELLING OF THE DIFFUSER

The geometry that will be used for the diffuser is adopted from the geometry used by Abbood A.H. [10] where the diffuser was modelled using GAMBIT. The geometry and the vertices of the diffuser is shown in Figure 6.1. For the numerical analysis to be done in FLUENT, an extension of 50% of the diffuser length of the numerical domain is necessary to prevent the occurrence of excessive reversed flow at the outlet. [7]



Note: Drawing not according to scale, and the dimensions are in metres

Figure 6.1: Diffuser geometry with vertices

The boundary of the diffuser inlet is set to be ‘PRESSURE FAR FIELD’, outlet is set to be ‘PRESSURE OUTLET’ and the upper and lower wall is set as ‘WALL’.

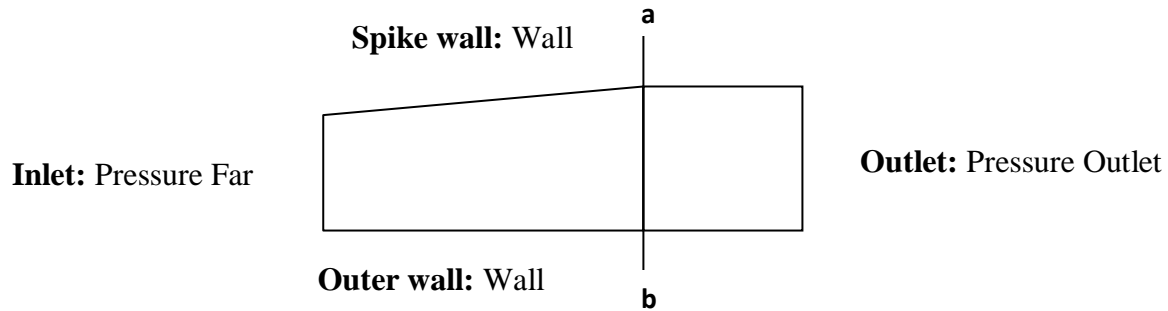


Figure 6.2: Boundary types of the diffuser

For the grid generations using GAMBIT, meshes of 40x120 grids are generated by using quadrilateral cells. The analysis of choosing the grids were performed by Tan Kien Weng where he compared 3 different types of meshes which are 40x120, 50x150 and 60x180. The three meshes are tested under the same input and the results below were found.

Mesh Name	Mesh Size	P_e (kPa)	$P_e/P_{o\infty}$	Ref($P_e/P_{o\infty}$)	% Error
M1	40x120	109.734	0.7207	0.745	3.26
M2	50x150	109.709	0.7205	0.745	3.29
M3	60x180	109.924	0.7219	0.745	3.1

Table 6.1: Pressure Recovery for different mesh sizes [7]

Since the error percentages are not very different and are below 5%, thus M1 is chosen as it contains lower number of meshes and the computations are faster.

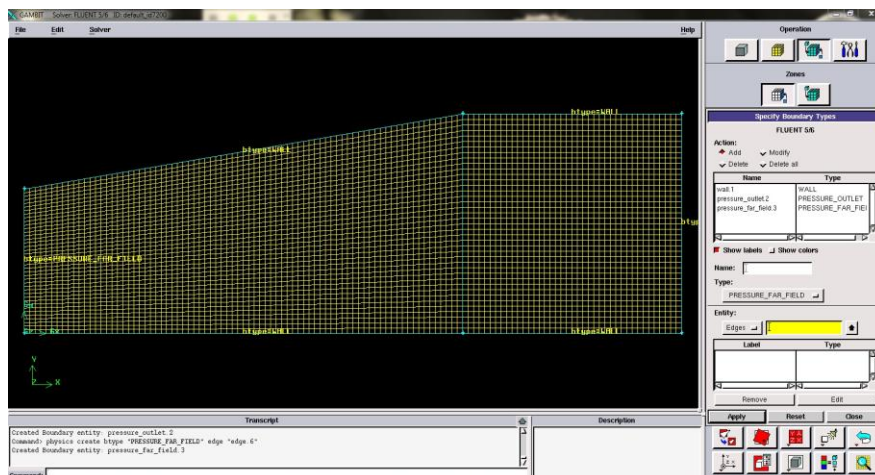


Figure 6.3: Diffuser inlet grid (40 x 120 quadrilateral cells)

6.2 MODELLING OF THE WHOLE SYSTEM

Modelling of the whole system is also done using GAMBIT. For this there will be a concentrated mesh at the area of where there will be a need of high numerical analysis and at the other parts the number of meshes will be reduced to reduce the duration of analysis. As per this, the meshing from the previous part will be used for the main system area and one half the numbers of meshes will be used at other area.

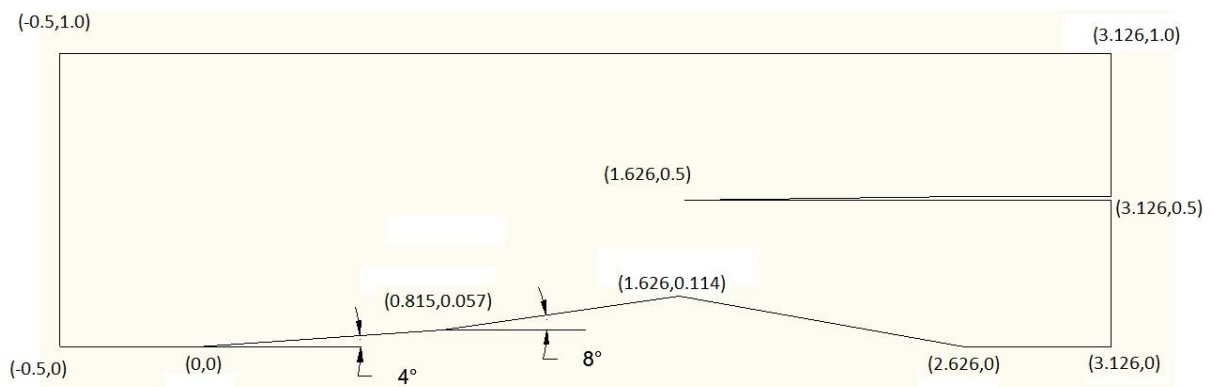


Figure 6.4: Whole system geometry

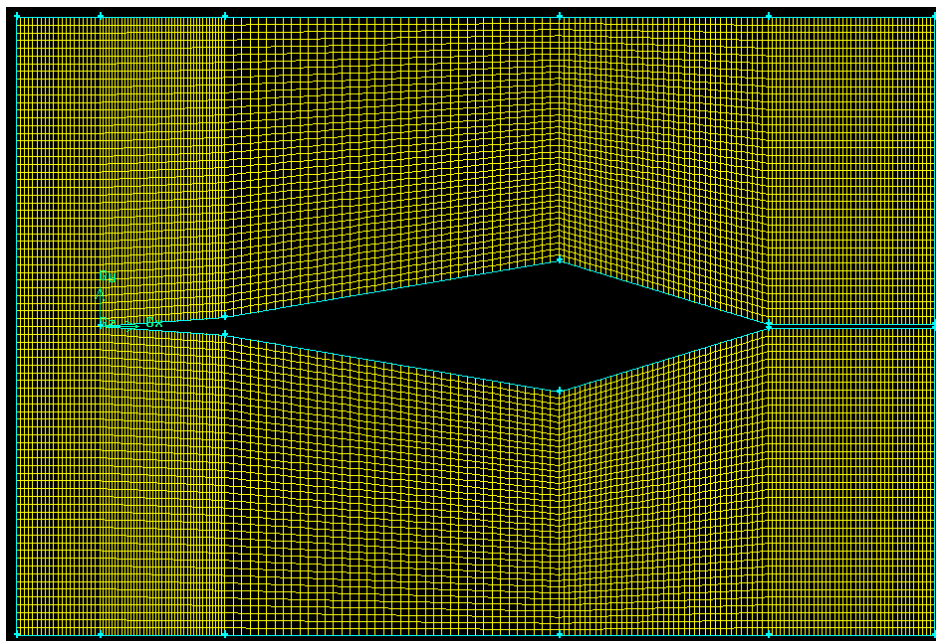


Figure 6.5: Grid and mesh generation for the whole system

6.3 RESULTS FROM NUMERICAL ANALYSIS FOR DIFFUSER FLOW

6.3.1 Results Comparison with Previous Numerical Work

To verify the results obtained in this study, a comparison has to be done with a previous work to verify the results. As for that, results from Tan Kien Weng [7] will be used as a comparison as the study used a similar method just a different geometry.

For the comparison, the pressure recovery at leeside and windward side vs angle of attack from this study will be compared to an earlier study [7]. The comparison is done with geometry of constant single wedge angle 6° . From the comparison done, as shown in Figure 6.6 and 6.7, we can see that the deviation is less than 10%. Thus, the results can be verified as correct. The reason for the deviation is because of the difference in geometry, where the current system uses a double wedge intake and the earlier system used a single wedge intake. The current system is supposed to yield better results as there is two oblique shocks.

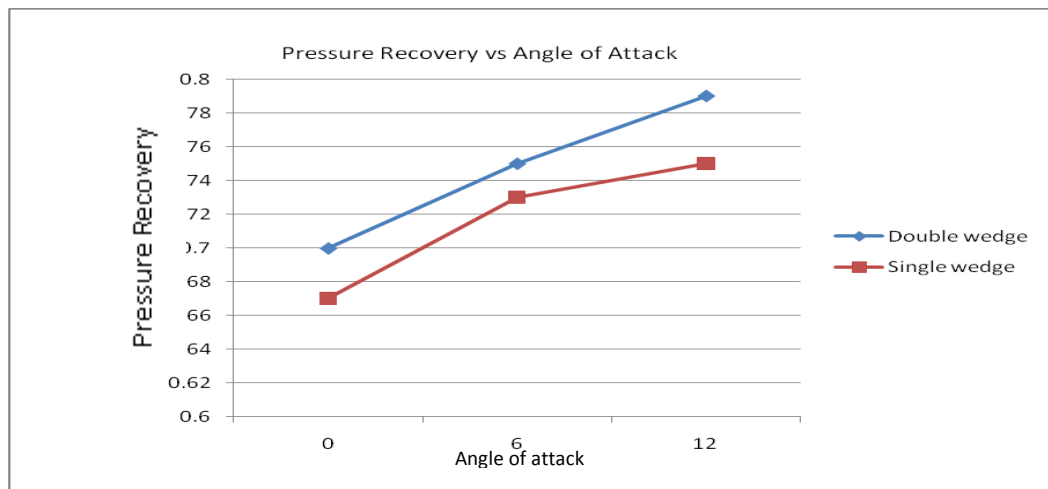


Figure 6.6: Results comparison at windward side for Ma=2.2

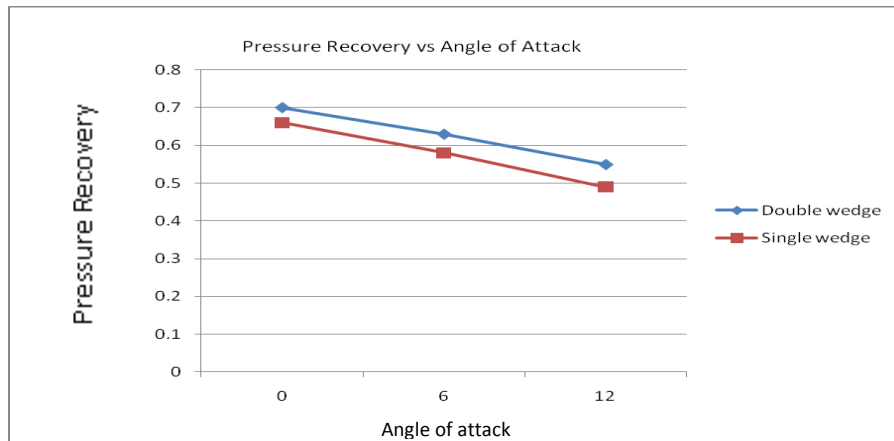


Figure 6.7: Results comparison at leeside for Ma=2.2

6.3.2 Effect of Mach Number and Angle of Attack on the Supersonic Jet Intake

This study has been conducted to analyse the effect of using double wedge spiked intake for a supersonic jet engine at different Mach No and angle of attack. It has shown effects on the pressure recovery.

Figure 6.8 shows the pressure recovery on the windward side of the supersonic intake by increasing the angle of attack for various Mach numbers. The results show that the body compression increases with the increase in the Mach No. The reason is due to the increase in angle of attack reflect in the increase in angle of attack, thus leading to a stronger shock wave which signifies higher compression.

Figure 6.9 shows the pressure recovery in the leeside of the supersonic intake by increasing the angle of attack for various Mach numbers. The results exhibit the behaviour whereby loss of body compression occurs as the angle of attack is increased. This is due to existence of Prandtl-Meyer behaviour and the reduction of angle of attack.

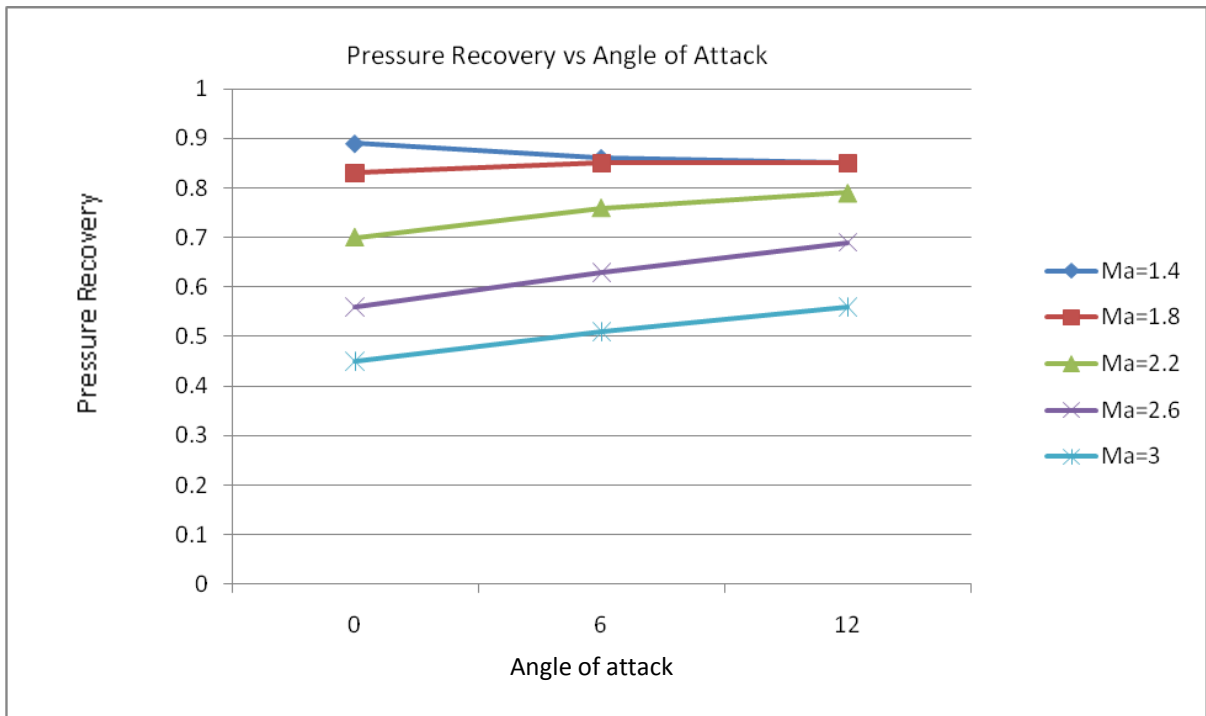


Figure 6.8: The effect of angle of attack on the pressure recovery at windward side

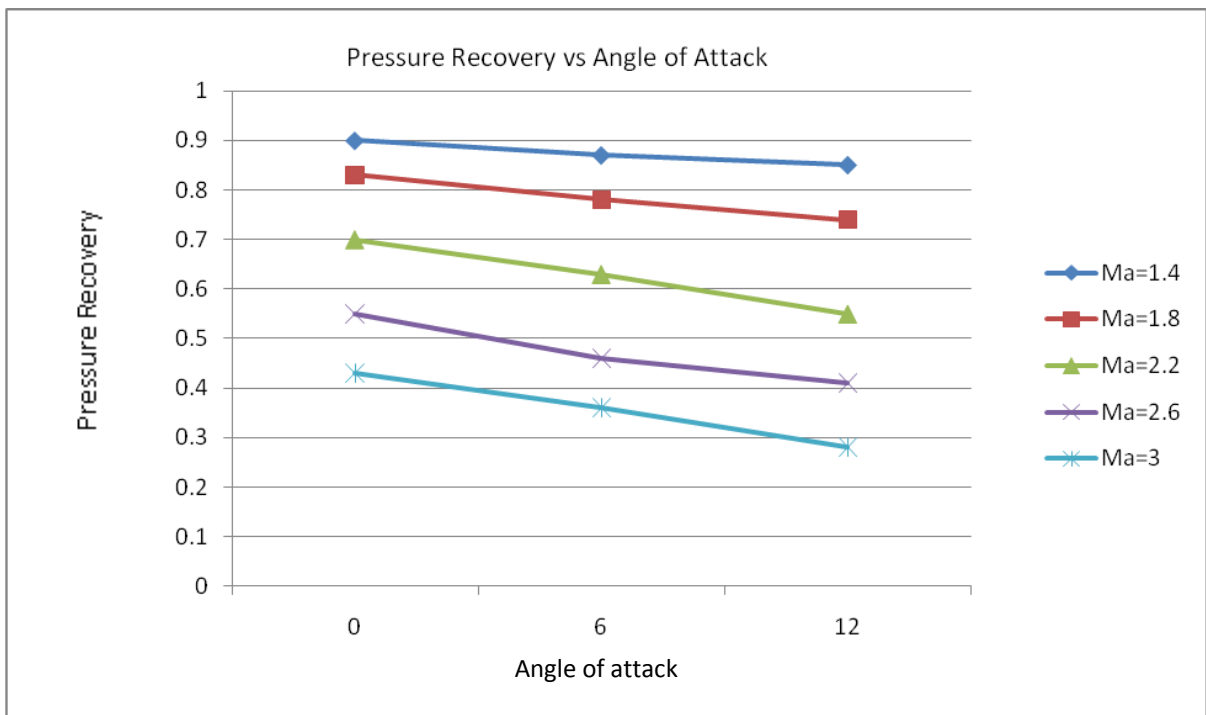


Figure 6.9: The effect of angle of attack on the pressure recovery at leeward side

6.3.3 Static Pressure Contour for the Diffuser Modelling

The contour of static pressure for both sides of the diffuser has been modelled and simulated. The contour shown are done for the $Ma=2.2$ with different angle of attacks ($\delta=0^\circ, 6^\circ, 12^\circ$).

The Figure 6.10 shows the contours at angle 0° and leeside and windward side. We can see that the contours are similar, because leeside and windward side experiences the same pressure recovery thus it is identical.

In Figure 6.11 and 6.12, the contours of static pressure for windward side and leeside at angle 6° and 12° are shown respectively. As can be seen, the difference in deflection angle will cause the pressure distribution at the leeside and windward side to be different.

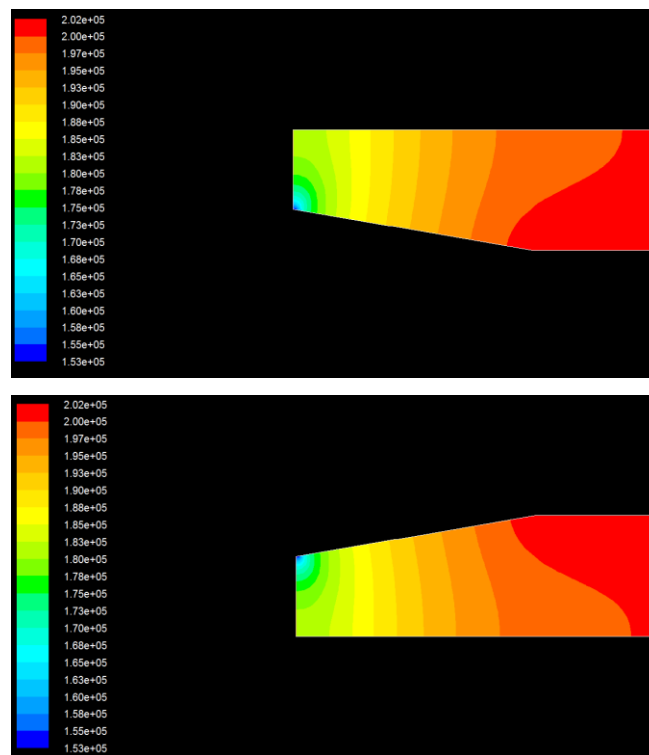


Figure 6.10: Contour of Static Pressure at Windward side and Leeside for $Ma=2.2$ and $\delta=0^\circ$

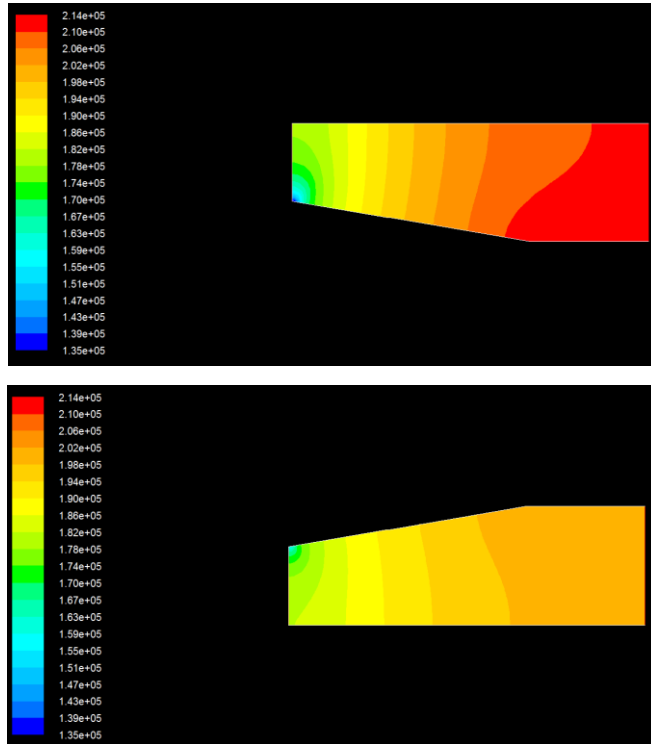


Figure 6.11: Contour of Static Pressure at Windward side and Leeward side for $Ma=2.2$ and $\delta=6^\circ$

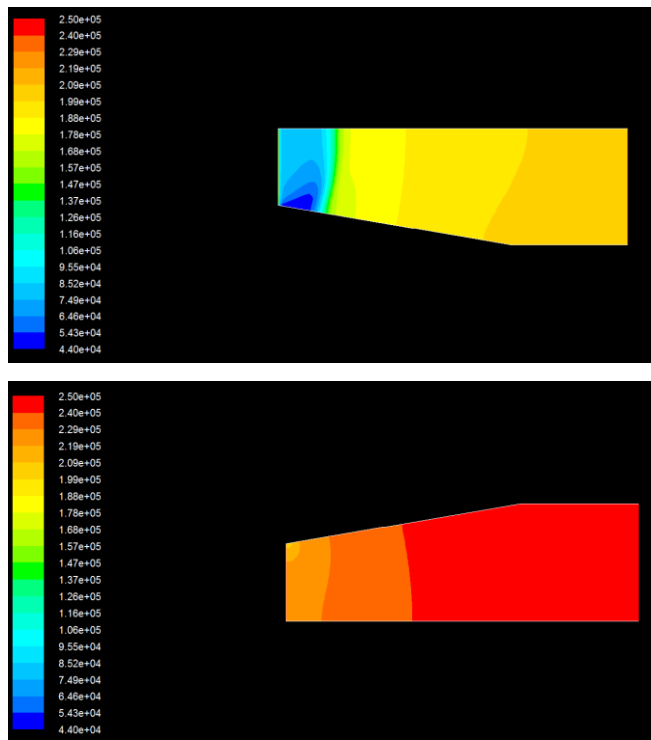


Figure 6.12: Contour of Static Pressure at Windward side and Leeward side for $Ma=2.2$ and $\delta=12^\circ$

6.3.4 Static Temperature Contour for the Diffuser Modelling

The contour of static temperature for both sides of the diffuser has been modelled and simulated. The contour shown are done for the $Ma=2.2$ with different angle of attacks ($\delta=0^\circ$, 6° , 12°).

The Figure 6.14 shows the contours at angle 0° and leeside and windward side. We can see that the contours are similar, because leeside and windward side experiences the same temperature variation.

In Figure 6.15 and 6.16, the contours of static temperature for windward side and leeside at angle 6° and 12° are shown respectively. As can be seen, the difference in deflection angle will cause the pressure distribution at the leeside and windward side to be different.

As can be seen, the temperature in the inner wall is higher compared to the outer wall. This is due to the flow slowing down faster at the spike wall compared to the outside wall.

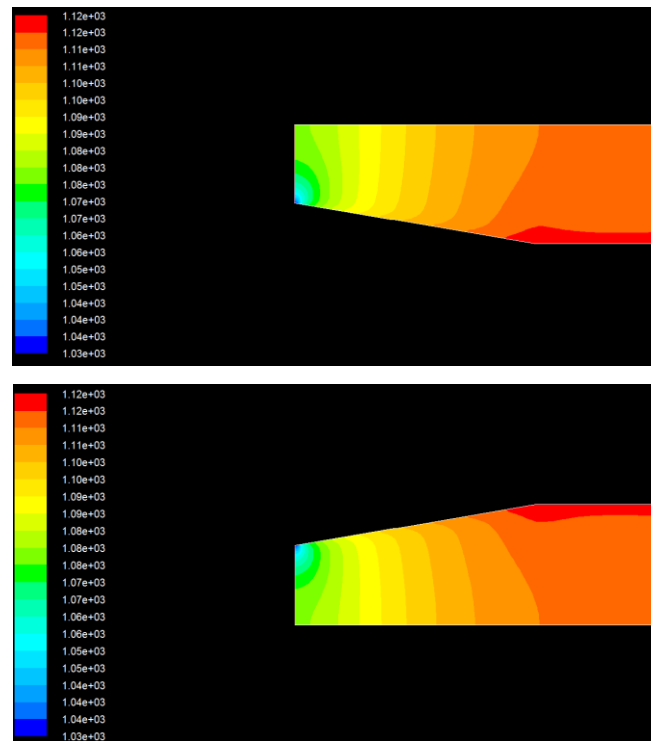


Figure 6.13: Contour of Static Temperature at Windward side and Leeside for $Ma=2.2$ and $\delta=0^\circ$

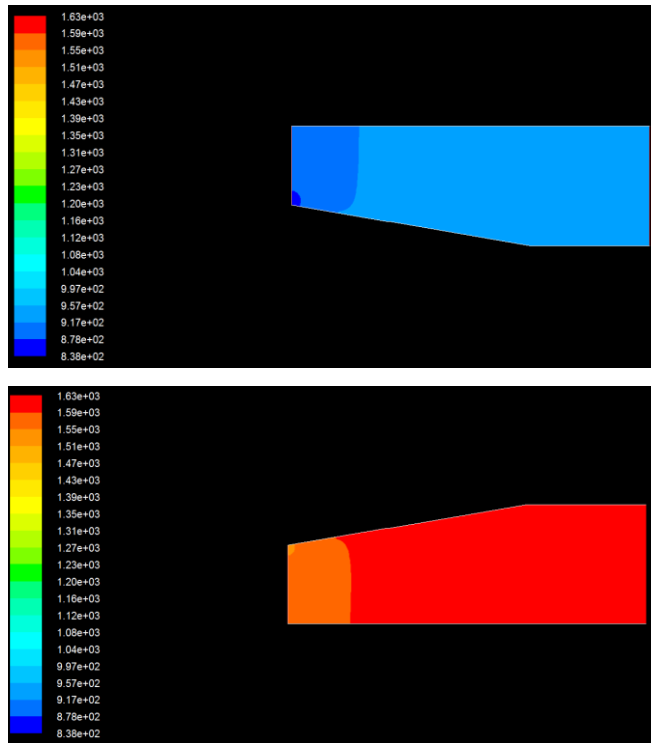


Figure 6.14: Contour of Static Temperature at Windward side and Leeside for Ma=2.2 and $\delta=6^\circ$

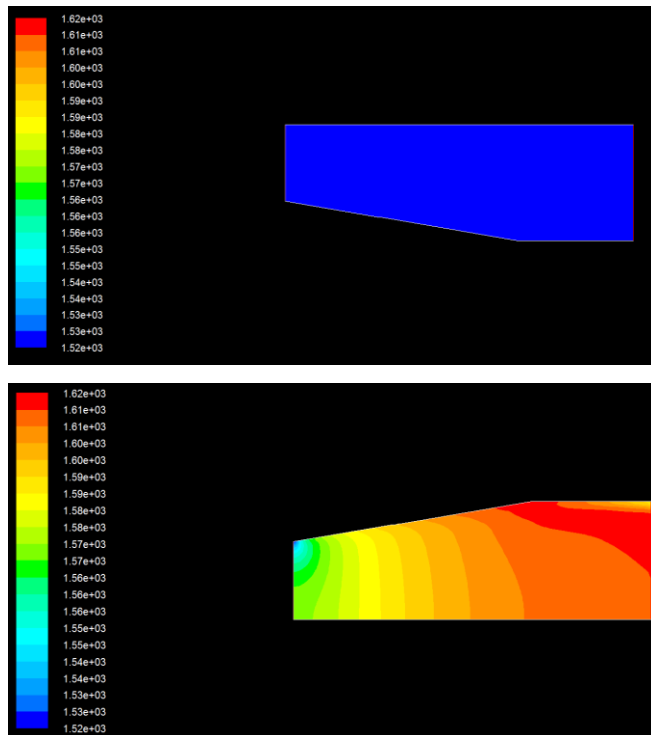


Figure 6.15: Contour of Static Temperature at Windward side and Leeside for Ma=2.2 and $\delta=12^\circ$

6.3.5 Velocity Magnitude Contour for the Diffuser Modelling

The figures show the velocity distribution for leeside and windward side for different angle of attack for $Ma=2.2$. We can see that at the region close to the wall, the velocity is zero. This is due to the non-slip condition of the surface.

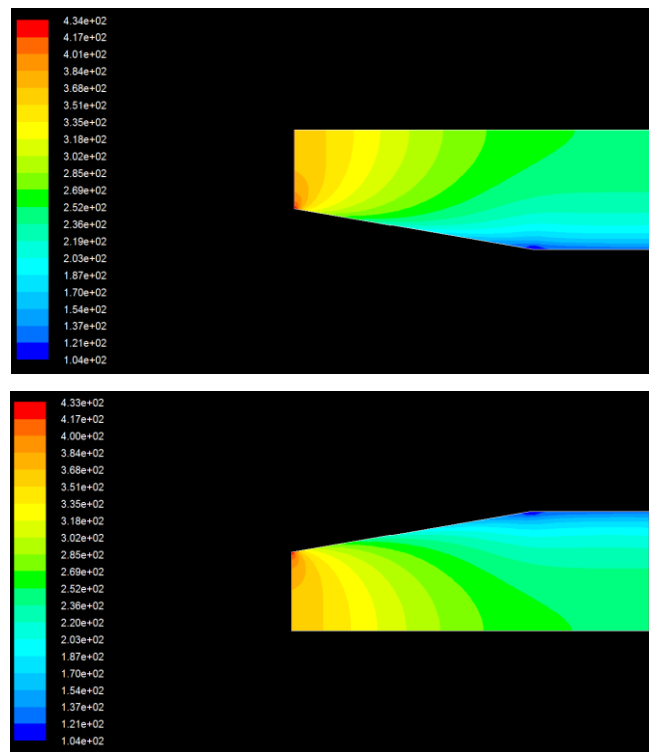


Figure 6.16: Contour of Velocity Magnitude at Windward side and Leeside for $Ma=2.2$ and $\delta=0^\circ$

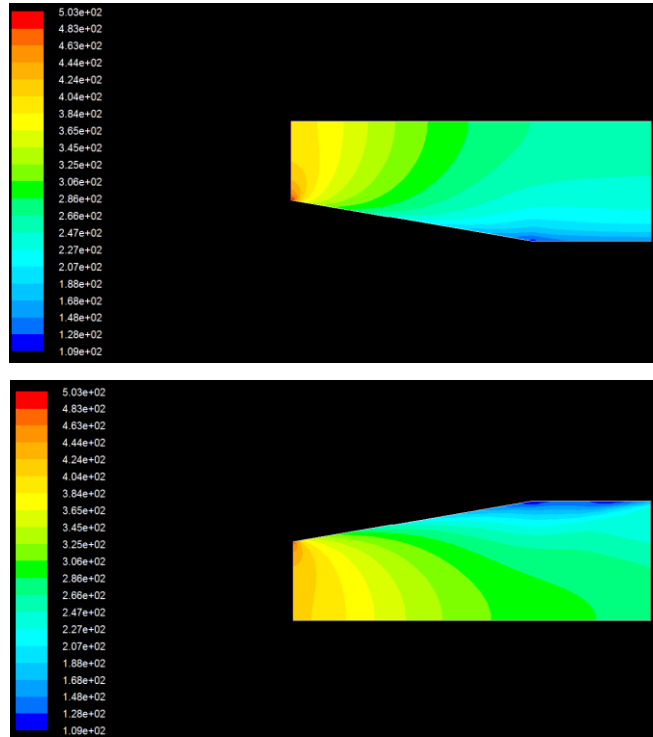


Figure 6.17: Contour of Velocity Magnitude at Windward side and Leeward side for Ma=2.2 and $\delta=6^\circ$

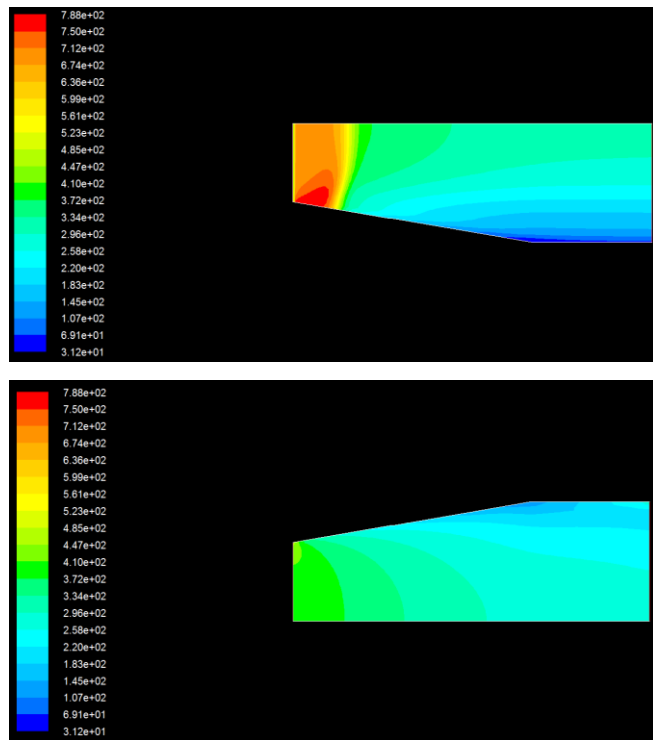


Figure 6.18: Contour of Velocity Magnitude at Windward side and Leeward side for Ma=2.2 and $\delta=6^\circ$

6.4 RESULTS FROM NUMERICAL ANALYSIS FOR WHOLE SYSTEM

6.4.1 Results Comparison with Different Mesh

There were several number of meshing were done for the whole system, from mesh spacing 0.1 to 0.3 with 0.05 increment. The grid was then run for the simulation, and all of it yielded the same results. The results are shown in appendix.

However, the difference is the number of iterations needed before convergence. The table shows the number of iterations before convergence.

Mesh Spacing	Number of iterations to convergence
0.1	1236
0.15	348
0.2	348
0.25	1139
0.3	216

Table 6.2: Result comparison for whole system simulation

6.4.2 Static Pressure Contour for the Whole System Modelling

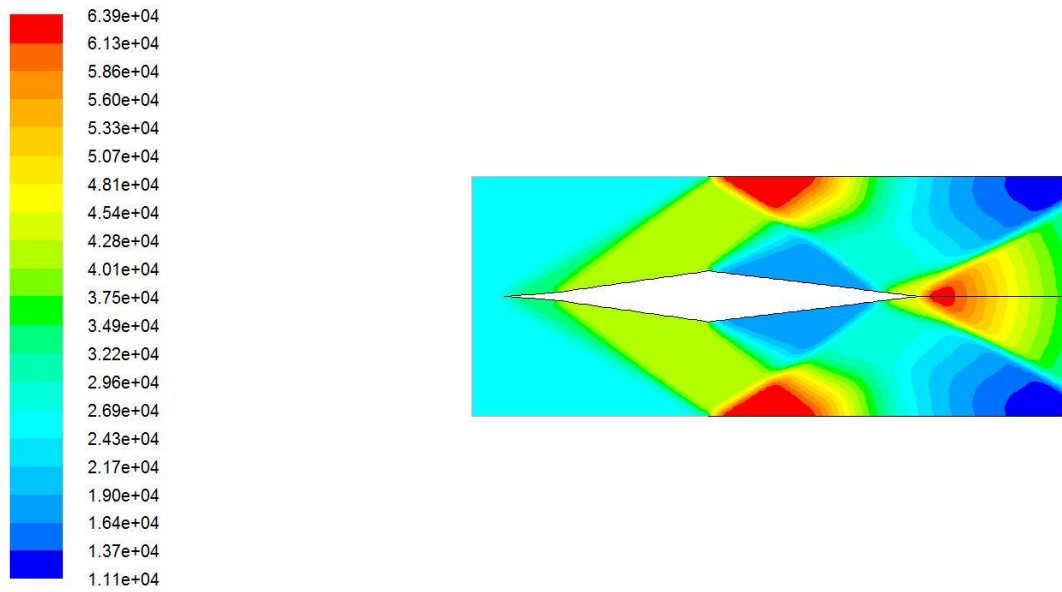


Figure 6.19: Contour of Static Pressure for $Ma=2.2$ and $\delta=0^\circ$

CHAPTER 7

CONCLUSION

The simulation on the double-wedge spike intake of the supersonic jet engine is a quite complex analysis. At zero angle of attack, the flow will go through two oblique shock waves at different shock angles before flowing through the normal shock waves. Then it goes through a diffuser before entering the compressor face. The shock waves part is analysed analytically and the diffuser part is analysed numerically, which is using FLUENT and GAMBIT.

6.1 CONCLUSIONS

From the analysis which has been done, we can see that pressure recovery increases with the angle of attack at the windward side and decreases with angle of attack at leeward side. Results also show clearly that the pressure recovery increases at both windward side and leeward side with the increase of Mach number.

The numerical simulation was performed successfully. The result that was obtained agrees with the previous results as shown in the comparison. The simulation was able to characterize the supersonic intake and the pressure recovery at the face of the compressor was predicted with a good accuracy. The simulation was also able to characterize the temperature and velocity distribution in the diffuser.

The numerical analysis was also able to capture the characteristics of the properties when the whole system, including the shock wave was simulated. The numerical analysis, FLUENT was able to capture the shock waves. However, the normal shock was not simulated as predicted. There were some contradictions of the numerical system with the analytical analysis.

Finally, we can conclude that having two series of oblique shock is able to increase the total pressure recovery thus improving the system. However, the system is not very effective to be used with low Mach number flights. Its efficiency increases as the flight speed increases.

6.2 RECCOMENDATIONS FOR FUTURE WORK

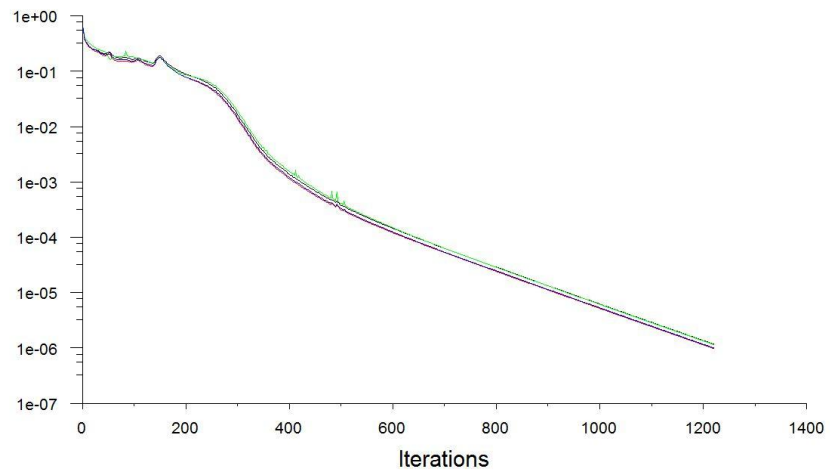
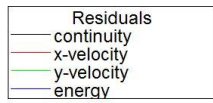
As this project has been completed, more studies should be done to understand the system more. As for a start, this project was done with a fixed geometry angle where both the wedge angles were 4° . The next project should study the effect of double wedge spike with more angles involved.

REFERENCES

- [1] Klaus Hunecke (1997), "Jet Engines: Fundamentals of Theory Design and Operation", Airlife Publishing LTD
- [2] D. Beastall (1956), "Flow Instability of Centre-body Diffusers at Supersonic Speeds", Aeronautical Research Council Reports and Memoranda, <http://aerade.cranfield.ac.uk/ara/arc/rm/2933.pdf>, 12/08/09
- [3] T.Wesmi M. Salih(2002), "The Flow Analysis of the Spiked Supersonic Intake", Msc. Theses, the college of Engineering Al-Mustansirirs University, Iraq
- [4] G.Raja Singh Thangadurai, B.S. Subhash Chandra, v. Babu and T. Sundararajan (2004), "Numerical Investigation of the Intake Flow Characteristics for a Ramjet Engine with and without Heat Addition in the Combustion Chamber:", Defense Science Journal, Vol.54, No.1, pp.3-16
- [5] Al-Kayiem H.H. and Aboud A.S (2007), "Flow Analysis in Spiked Supersonic Intakes of A/C (I-Inviscid)", Platform UTP, Volume Five, Number Two, July-December 2007 issue.
- [6] http://en.wikipedia.org/wiki/Jet_engine; 12/08/09
- [7] Tan Kien Weng (2009), "Simulation and Flow Characterization of Spiked Supersonic Gas Turbine Intake at Non-Zero Angle of Attack", Final Year Project, Universiti Teknologi PETRONAS, Malaysia
- [8] Dr. Hussein H. Al-Kayiem and T. Wesmi M. Salih, "The Effect of Incidence and Forebody Angles on the Performance of Spiked Supersonic Intake", Baghdad, Iraq
- [9] M.K. Jain & S.Mittal (2005), 'Euler Flow in a Supersonic Mixed-Compression Inlet', International Journal for Numerical Methods in Fluids

- [10] Abbood A.H. (1999), 'Numerical Analysis of Two-Dimensional Convergent-Divergent Nozzle for a Modern Fighter'. Msc. Thesis, the college of Military Engineering.
- [11] Yunus A. Cengel and John M. Cimbala (2006), 'Fluid Mechanics', McGraw-Hill Company
- [12] Robert W. Fox, Alan T. McDonald, Philip J. Prithchard (2004), 'Introduction to Fluid Mechanics, John Wiley & sons, Inc.
- [13] <http://www.grc.nasa.gov/WWW/K-12/airplane/mshocka.html>, 17/3/2010

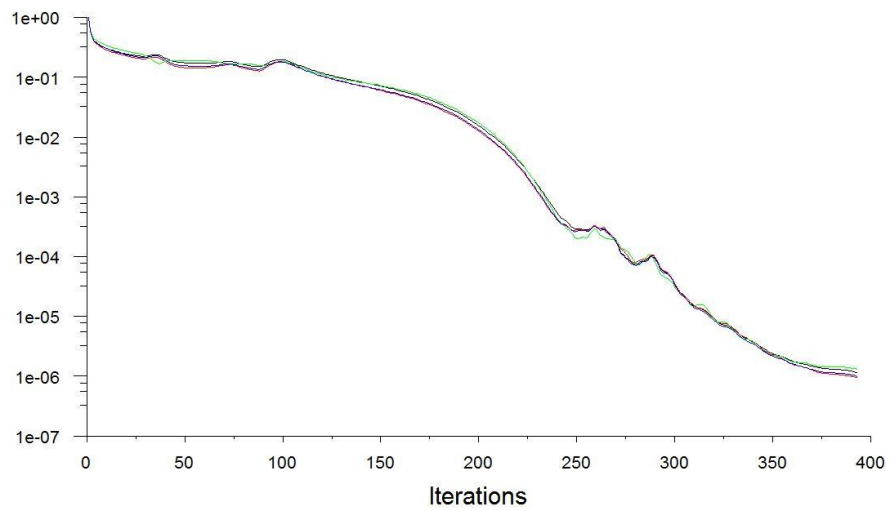
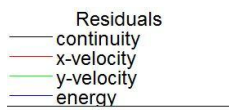
Appendix



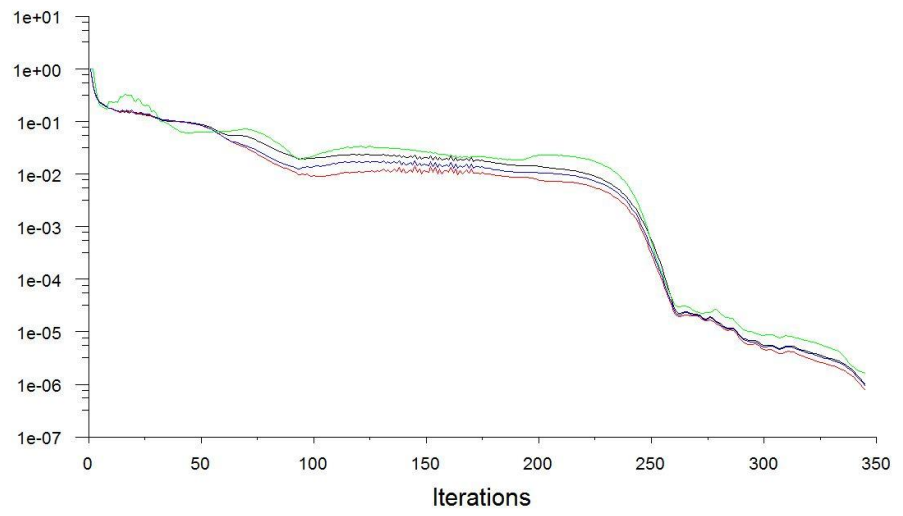
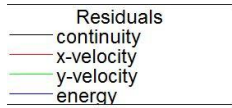
Scaled Residuals

May 27, 2010
FLUENT 6.3 (2d, dp, dbns imp)

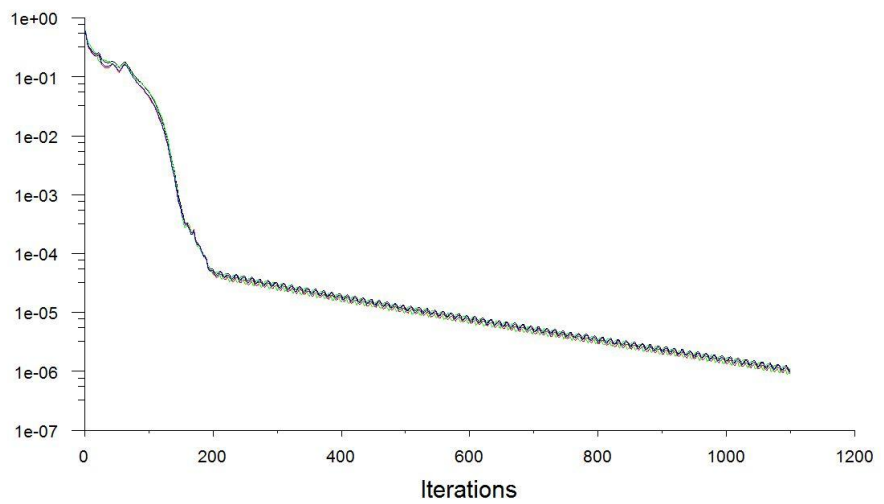
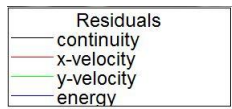
0.1 Mesh Spacing residual



0.15 Mesh Spacing residual

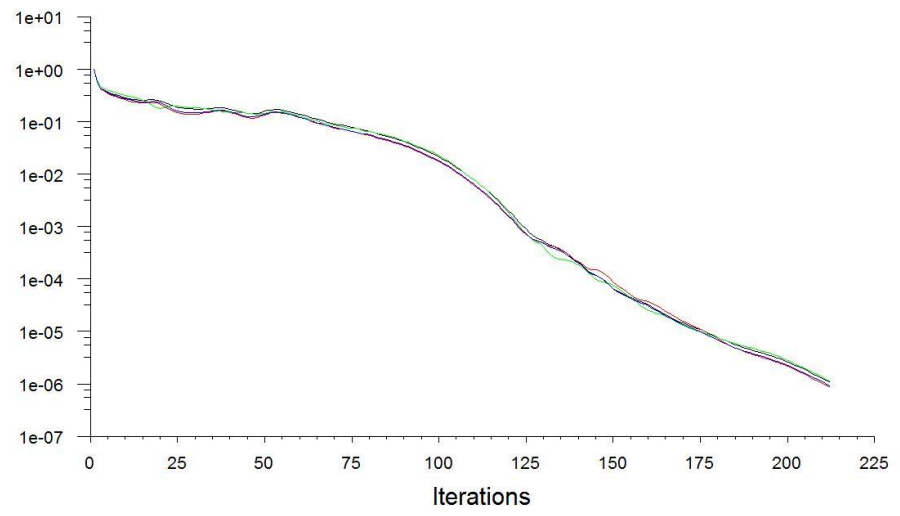


0.2 Mesh Spacing residual



0.25 Mesh Spacing residual

Residuals
— continuity
— x-velocity
— y-velocity
— energy



0.3 Mesh Spacing residual